Chapter 6

Additive Manufacturing of Ti-Alloys for Aerospace, Naval and Offshore Applications

Chapter details

Chapter DOI:

https://doi.org/10.4322/978-65-86503-83-8.c06

Chapter suggested citation / reference style:

Mendoza, Michael Y., et al. (2022). "Additive Manufacturing of Ti-Alloys for Aerospace, Naval and Offshore Applications". *In* Jorge, Ariosto B., et al. (Eds.) *Fundamental Concepts and Models for the Direct Problem,* Vol. II, UnB, Brasilia, DF, Brazil, pp. 154–183. Book series in Discrete Models, Inverse Methods, & Uncertainty Modeling in Structural Integrity.

P.S.: DOI may be included at the end of citation, for completeness.

Book details

Book: Fundamental Concepts and Models for the Direct Problem

Edited by: Jorge, Ariosto B., Anflor, Carla T. M., Gomes, Guilherme F., & Carneiro, Sergio H. S.

Volume II of Book Series in:

Discrete Models, Inverse Methods, & Uncertainty Modeling in Structural Integrity

Published by: UnB City: Brasilia, DF, Brazil Year: 2022

DOI: https://doi.org/10.4322/978-65-86503-83-8

Additive Manufacturing of Ti-Alloys for Aerospace, Naval and Offshore Applications

Michael Y. Mendoza[1*], Leonel Leonardo Delgado - Morales[2], and Victor Contreras Palma[3]

[1*]Institute of Naval Architecture and Ocean Engineering, Universidad Austral de Chile,
E-mail: michael.mendoza@uach.cl
[2]Institute of Design and Industrial Methods, Universidad Austral de Chile, Chile.
E-mail: leonel.delgado@uach.cl
[3]Institute of Naval Architecture and Ocean Engineering, Universidad Austral de Chile.
E-mail: victor.palma@uach.cl
[*]Corresponding author

Abstract

Titanium alloys are well-known by their excellent corrosion resistance and high strength-to-weight ratio. The aerospace industry has been taking advantage of those properties and enhancing them with novel manufacturing techniques such as Additive Manufacturing (AM). However, the naval and offshore industry has very limited use of those benefits. This is mainly due to technical limitations such as small-scale parts and low deposition rates of the most common AM processes. This work presents a review of the state-of-the-art in AM and its applications, in which relevant publications related to this important area of investigation are considered. Initially, titanium is described as the main alloy. The Laser Engineered Net-Shape (LENS™), Electron Beam Additive Manufacturing (EBAM®) and Wire Arc Additive Manufacturing (WAAM) processes are presented. Given that WAAM offers potential solutions for size and deposition rates with design challenges and new materials for component fabrication, at the end of the chapter, applications from the naval and offshore areas where this method is used are shown.

Keywords: Titanium alloys; additive manufacturing; naval and offshore industry; aerospace components; WAAM

1 Introduction

Titanium alloys are recognized by their excellent mechanical and chemical properties such as excellent corrosion resistance, good fatigue performance and low modulus (high flexibility). Several examples of Ti-alloys applications are aircraft components, automotive, chemical processing equipment, biomedical industries and more recently in naval applications. During titanium processing, an inert atmosphere or vacuum is required, and this condition among others becomes titanium a material of high cost. Therefore, certain applications have limitations to use this material

(Lütjering and Williams [2007]). To justify the inherent cost of titanium, features and characteristics of novel techniques as additive manufacturing (AM) need to be deeply understood to take advantage of the processing methods and the resultant material properties.

Additive manufacturing of titanium alloys has several applications as mentioned before. However, the focus has been in the aerospace industry and more specifically for military applications. A common limitation for AM is the part size. Most AM techniques focus on small processing chambers to produce small parts. The naval industry is characterized by large-size components, but it has been working gradually to use parts made by AM (Ziółkowski and Dyl [2020]). The global market is increasing the use of additive manufacturing technology and the titanium demand. Figure 1 shows the US market projection until 2028. Therefore, it is important to understand material processing conditions, microstructure, and performance correlation (Londono [2019]).

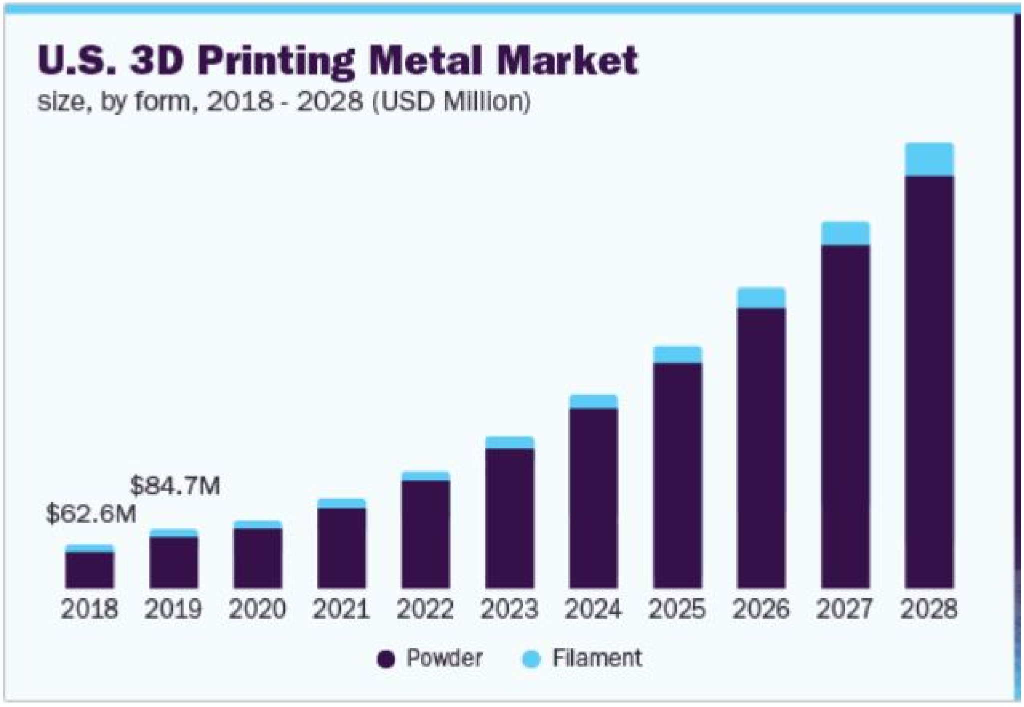

Figure 1: U.S. AM Metal Market (Grand View Research Inc [2021])

This chapter discusses additive manufacturing technology in general and focuses on laser engineered net-shape (LENS$^{\textbf{TM}}$), electron beam additive manufacturing (EBAM$^{@}$) and wire arc additive manufacturing (WAAM). Titanium alloys will be the main material, but other materials will be also analyzed. The discussion will also include specific applications on aircraft, naval and offshore components.

2 Titanium Alloys

Elemental titanium is hexagonal closed packaged structure (HCP) also known as α phase. P6$_{3/mmc}$ is the space group symmetry with number 194. As an allotropic metal, titanium transforms at 882°C to body-centered cubic structure (BCC) also known as β phase. Im$\overline{3}$Ìm is the space group symmetry with number 229 (Lütjering and Williams [2007]). Figure 2 shows those 2 crystal structures with lattice parameters and the most close-packed slip planes.

The α phase has a c/a ratio of 1.587 which is lower than the ideal of 1.633. It makes the prism slip planes more packed than the basal slip planes. The β phase to the right of Figure 2 shows a

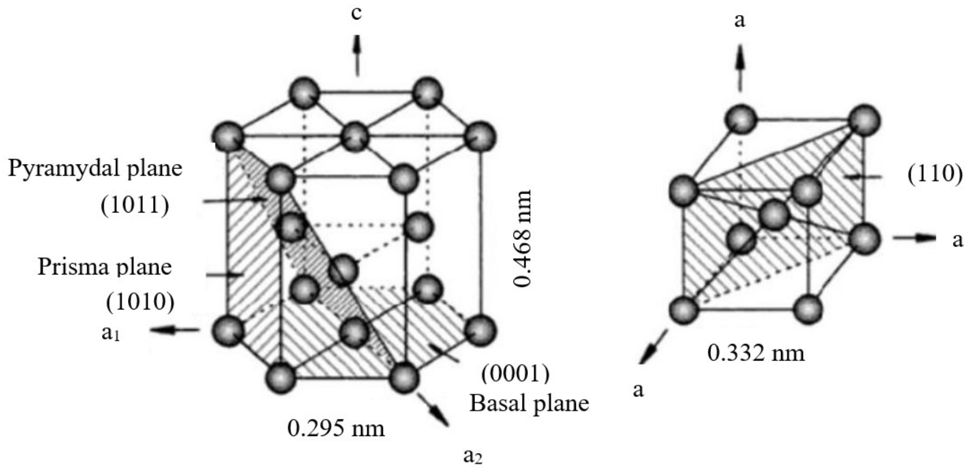

Figure 2: Crystal structure of phase (left) and β phase (right) (Londono [2019])

lattice parameter of 0.332 nm which is at 900°C (Lütjering and Williams [2007]). The Youngâ modulus in single crystals of α is from 100 Gpa with a stress axis perpendicular to the c-axis and 145 Gpa with a stress axis parallel to the c-axis. This fact shows the high elastic anisotropy of pure titanium at room temperature. The Youngâs modulus in single crystals of β phase can not be measured due to the instability of that phase at room temperature. The β phase can be stable at room temperature just by addition of alloying elements (Londono [2019])

2.1 Alloying elements

The purpose to add another element to titanium is to stabilize either α phase or β phase. This is achieved by changing the position of the α/β transformation temperature. Figure 3 shows schematic diagrams of the most common alloying elements of titanium. Al, O, N and C are α stabilizers. It means they rise the α/β transformation temperature. Al is the most common α stabilizer due to its high solubility. Oxygen content can affect the strength of titanium and it is used to define different grades of commercially pure (CP) titanium. Other elements as B and Ge can stabilize α phase, but their solubilities a lower and can form intermetallic compounds (Lütjering and Williams [2007]). The alloying elements that stabilize β phase can be isomorphous which means they are miscible at all compositions or eutectoid that basically means they are not miscible at all compositions and can form other phases. Examples of β isomorphous stabilizers are V and Mo. Vanadium being used in the most common Ti-alloy Ti-6Al-4V.

Fe, Cr and Si are common β eutectoid stabilizers. There are some other elements as Zr and Sn that are considered neutral. α titanium alloys are common in the chemical and processes industry where corrosion resistance and ductility are required. On the other hand β titanium alloys are largely utilized in biomedical applications due to their biocompatibility and low modulus (Chen et al. [2020]). However, it is important to mention that most of the commercial alloys are multicomponent. Ti-6Al-4V is the best example of a multicomponent alloy and it is known as the âworkhorseâ of the titanium industry with more than 50% of the total titanium usage of the world (Inc [2022]).

2.2 Alloy classification

Titanium alloys are classified based on the metallurgy. In other words, it is based on the final microstructure. There are alpha (α), near alpha, alpha + beta (α+β) and beta (β) titanium alloys.

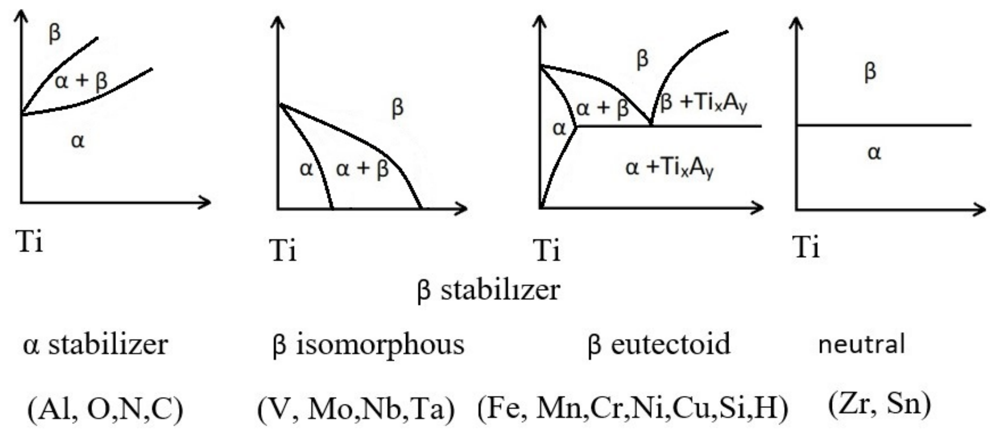

Figure 3: Schematic alloying elements effect on titanium (Lütjering and Williams [2007])

Each different microstructure offers different properties for different specific applications. Alpha and near alpha alloys have low and medium strength, which increases with the addition of interstitial elements or impurities such as Oxygen, Nitrogen or Carbon (Londono [2019]). The ASTM classify the commercially pure titanium alloys by CP Grade $'X'$. Where the grade is a number that indicates the oxygen content 0.18 wt% to 0.4 wt% for grades from 1 to 4 (NeoNickel [2022]). Table 1 shows the classification of titanium alloys with some examples.

Table 1: Commercial titanium classification

Titanium Classification	Titanium Grades
Alapha (α)	CP Grades 1,2,3,4
Near - alapha (α)	Ti-5Al-2.5Sn, Ti-3Al-2.5V
Alapha + Beta (α+β)	Ti-6Al-4V, IMI 685, IMI 834, Ti-811
Beta (β)	Beta 21S, Beta C, Ti-6246, Beta CEZ

The near-alpha alloys are mostly alpha, but with small amount of beta phase (2-5 vol.%) (Lütjering and Williams [2007]). These alloys are as alpha good for corrosion resistance applications, but the small amount of beta phase controls the recrystallization of α grains upon annealing. The α + β alloys have both phases, but β is present in a larger proportion than in the near α alloys. These alloys are heat treatable which means higher strength and hardness than α or near α alloys. However, creep strength and cold formability are not as good as for α alloys. These alloys are also classified by their microstructure into fully lamellar, equiaxed and bi-modal. The detailed description of those microstructures can be found in (Lütjering and Williams [2007]). Finally, β alloys are rich in β phase and are heat treatable to reach very high strength. However, fatigue strength and ductility in the heat-treated condition are low. Alloys such as Beta 21S and Beta C are mostly used in aerospace applications.

3 Additive Manufacturing

In general terms, additive manufacturing (AM) can be defined as a process where a heat source melts added material to a substrate. The heat source is in relative motion respect to the substrate to build the computer aid designed shape of the deposition. In Figure 4, common heat sources are presented (e.g., laser, electron beam and plasma). Also, all feedstocks are showed (e.g., wire, powder bed and powder blown) Collins [2003].

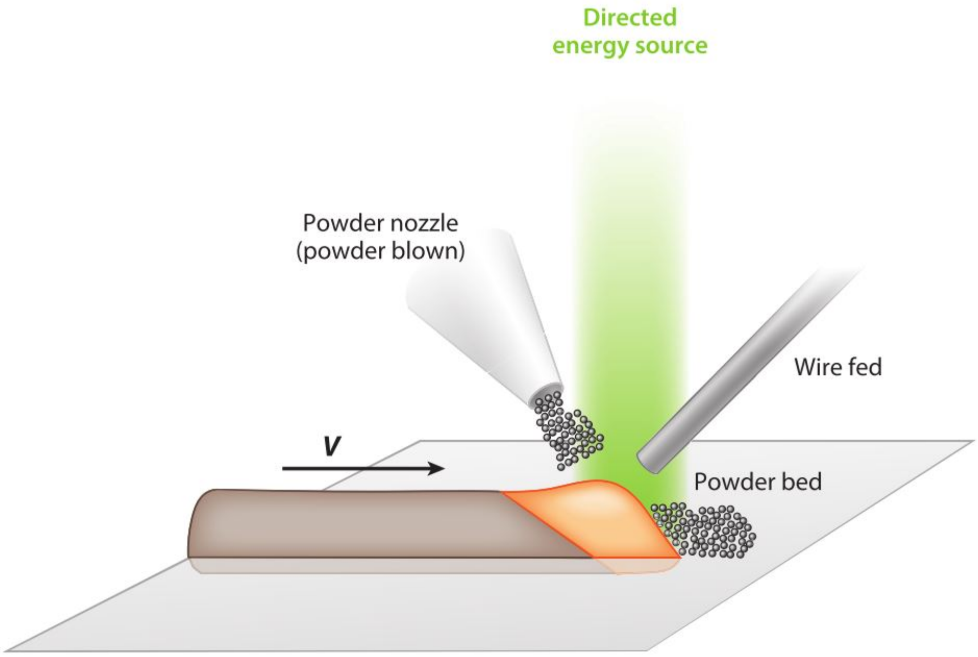

Figure 4: Schematic one pass of AM (Adapted from Collins [2003])

In addition, AM systems can be defined by the atmosphere where the process is occurring (e.g., inert gas, vacuum, and gas shield). AM technology has a strong influence on material properties due to the processing conditions such as heat source power, atmosphere, deposition speed among others. The microstructure is defined by heat transfer, fluid dynamics, phase transformations and the thermophysical properties of the material. Knowing the microstructure evolution in AM is very important to determine the properties of the material (Mendoza et al. [2019]). AM is a process that involves a condition that is far from thermodynamical equilibrium due to the rapid solidification. This factor leads to a lower solute partitioning compared with other manufacturing techniques (Collins et al. [2016]).There are several studies regarding the microstructure evolution of AM (Thijs et al. [2010] and Kriczky et al. [2015]). Some other studies have been focus on the molten pool modeling to predict the experimental microstructure evolution Peyre et al. [2008] and Rolchigo et al. [2017]). AM offers the research advantage of produce graded compositions within the same sample. This is achieved by using elemental powder blends in a system with multiple hoppers (Collins [2003] and Gong et al. [2017]).

The grain size in any microstructure is important for the resultant mechanical properties. There are many efforts to study the effect of alloying elements on grain size (Bermingham et al. [2008]). In 2001, a model was developed to predict the grain size refinement based on constitutional under-cooling and nucleant particles (Easton and St. John [2001]). Alloying elements such as boron (B) (Bermingham et al. [2008]) and beryllium (Be) (Bermingham et al. [2009]) acting as good grain refiners. All these efforts were focused on casting titanium alloys, but the fundamentals were extrapolated to additive manufacturing on titanium alloys for alloying elements such as molybdenum (Mo) (Mendoza et al. [2019]) and tungsten (W) (Mendoza et al. [2017]). More recent research revealed the grain refiner power of lanthanum oxide (La_2O_3) (Ng et al. [2022]) and an hydrogenation treatment on wire arc additive manufacturing (WAAM) (Xiaolong et al. [2022]).

Texture in additive manufacturing has been reported by many researchers in several alloys, including Ti-alloys (Banerjee et al. [2006]). Build orientation can affect the mechanical properties as reported by Simonelli (Simonelli et al. [2014]). In addition, many researchers have demonstrated how the processing parameters of additive manufacturing such as energy density or travel speed determine the microstructure (Hrabe and Quinn [2013]). In the classical understanding of solidification in AM, a <001> growth direction has been reported to be parallel to the maximum gradient of temperature (Mendoza Londono [2016]). This preferential direction on solidification (i.e., texture) creates the intrinsic anisotropy of some additive manufactured Ti-alloys. However, the common columnar microstructure in AM can be modified to equiaxed by the addition of alloying elements (Collins et al. [2016]) or by further heat treatments (Qi et al. [2021]).

4 Laser Engineering Net-Shaping (LENS^{TM})

In 1997, this technology was licensed by Optomec Inc. It was originally developed by Pratt Whitney and Sandia National Laboratories (Mudge and Wald [2007]). The heat source in this technique is a laser and the regulated flow of mass is controlled by a powder feed system. Argon gas atmosphere is used as protection and keeps oxygen content lower than 10 ppm in the glove box (Obielodan and Stucker [2012]). Several advantages of this technique include less machining required to the final component, it can repair or manufacture new components and different elements can be used at the same time (e.g., compositionally graded parts) (Mendoza Londono [2016]). Figure 5 shows the typical process lay-out.

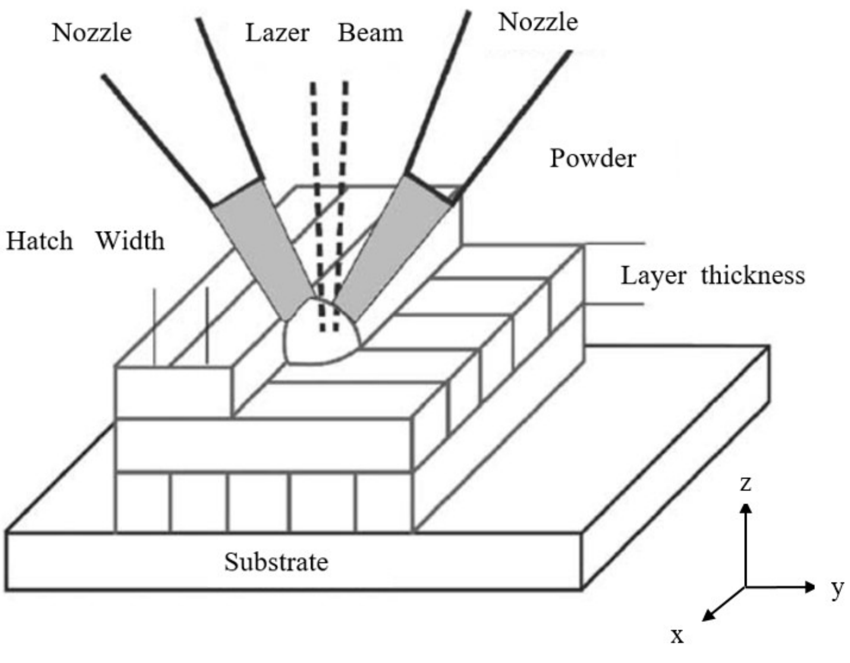

Figure 5: Schematic representation of LENS^{TM} process (Collins [2003])

In 2001 was reported the thermodynamic enthalpy of mixing as a key factor determining the compositional homogeneity and microstructure Schwendner et al. [2001]. Laser power and hatch width are LENS^{TM} parameters that can be modified independently to control the resultant microstructure of the deposited material. However, it was previously and conveniently demonstrated that all LENS^{TM} parameters are related to the total contribution of input energy. Therefore, travel speed, laser power, hatch width and layer thickness can be represented by a single term called energy density Sears [2002]. This term can be used to understand the resultant mechanical properties of the deposited material. In fact, at certain level of energy density the deposited material or component will show equivalent mechanical properties to a conventionally forged material of the same composition Collins [2003]. As an example the critical energy density for IN 690 N2 is 165 Wh/in^3 Sears [2002]. Timetal 21S (also known Beta-21S) is a β type titanium alloy with composition Ti-15Mo-2.7Nb-3Al-0.2Si in Wt.%. 15Mo was replaced by 9.4Cr which is the equivalent amount required to stabilize β phase in the same proportion than the 15Mo. Cr was selected because its enthalpy of mixing (Δ Hmix) with titanium is -32 kJ/mol compared with -16 kJ/mol for Ti-Mo. This replacement of alloying element demonstrated that the total input energy (energy density) can be altered by the enthalpy of mixing. In this specific case the higher exothermic enthalpy of mixing of Ti-Cr reduced the critical energy density by $\sim$ 3kJ/in^3 Collins [2003].

4.1 Discontinuities in LENS^{TM} deposits

Very acceptable processing parameters on LENS^{TM} have been determined by trial-and-error approach. However, several work has been done to establish the relationship between the resultant microstructure of deposited material and the processing parameters Kobryn et al. [2000] This understanding is very important for the process control and design. Discontinuities include porosity, lack of fusion between layers and unmelted particles. Porosity is caused by entrapment of gas from either the powder feed system or from the powder particles. The porosity reported is nearly spherical in shape and did not have any preferential location Kobryn et al. [2000].In general terms, the porosity will decrease inasmuch the power increases and it is related with the fact that more power is more energy available to melt the same amount of powder. However, a reduction of porosity because of a higher travel speed is not as intuitive as for the power supply. The explanation reported Kobryn et al. [2000] for this behavior is the reduction of delivered powder due to the augmented travel speed.

The entrapped gas bubbles come from the powder system or the powder itself as mentioned before. However, a very high input energy on a small area of material can produce a keyhole Courtois et al. [2014]. This physics phenomena results in a very deep and narrow shape of the molten pool and that shape makes more difficult to gas bubbles to escape from the solidification front. High levels of input energy can also contribute to molten pool instabilities and create spheroidization of the liquid metal, also known as balling effect Gu et al. [2013]. This balling effect can induce more porosity Attar et al. [2014]. Figure 6 shows a pore in a SEM image (a) and a schematic molten pool with entrapped gas bubbles (b).

Lack of fusion between layers is due to not enough energy to melt the previously deposited layer or the substrate for the first layer. This can be caused by low energy density or an excessive powder feed rate Liu et al. [2021]. It is also known that the substrate acts as a heat sink and according to Kobryn et al. thin substrates dissipate heat faster than thick substrates. This condition leads to thin substrates to show more lack of fusion compared to thick substrates (Kobryn et al. [2000]).

As mentioned at the beginning of this section all processing parameters in LENS^{TM} can be represented by the energy density term (Collins [2003]). This term is defined by Equation 1. Here ρ is the laser power, ν is the travel speed, $t_{thickness}$ is the layer thickness or spacing and $t_{thickness\ width}$ is the distance between passes (Mendoza et al. [2017]). The energy density is proportional with the grain width on the columnar morphology in LENS^{TM} depositions. Higher energy density values will produce larger molten pools, which in turn implicates lower cooling rates (Mendoza et al. [2017]). Figure 7 shows this trend for the Ti-W system.

$$\rho_{energy} = \frac{p}{\nu \cdot t_{thickness} \cdot t_{thickness\ width}}. \quad (1)$$

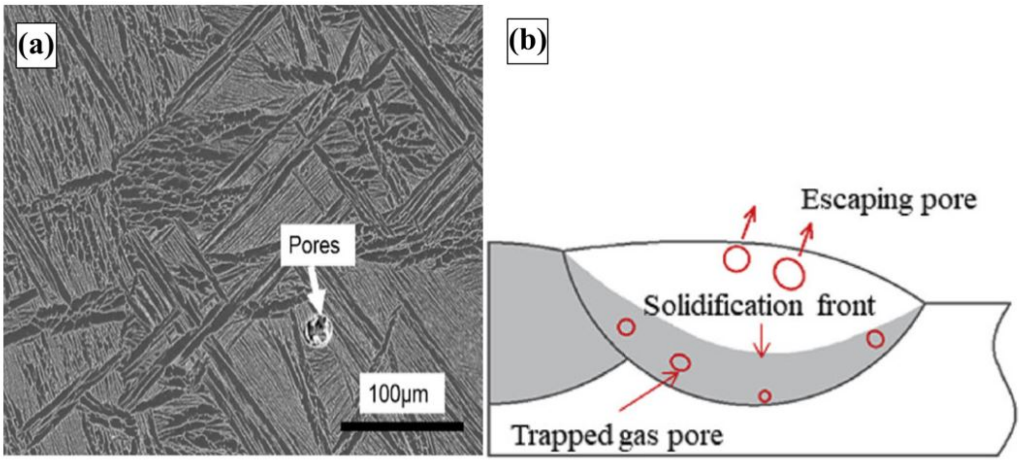

Figure 6: Pore in a Ti-alloy (a) and pores in molten pool (adapted from (Liu et al. [2021])

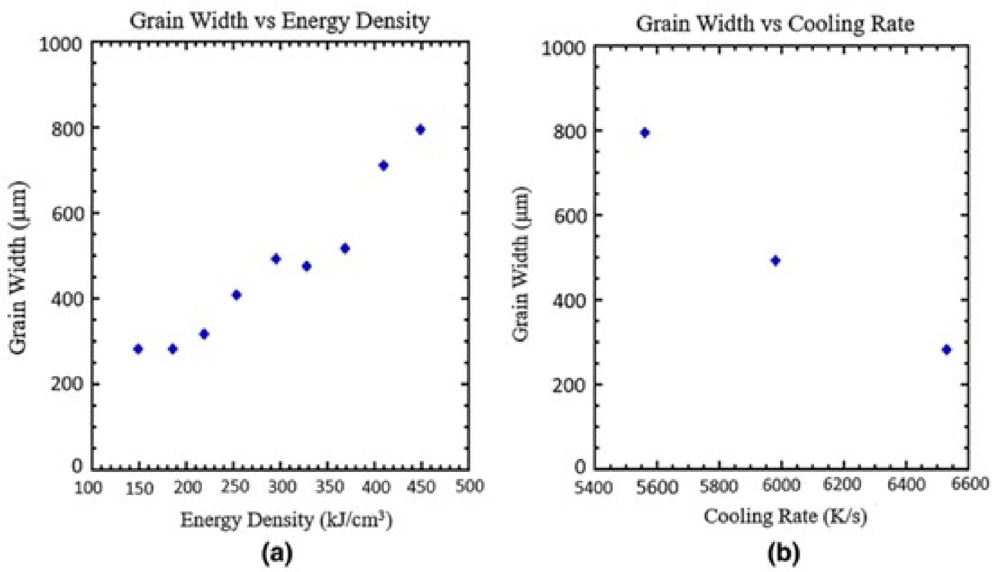

Figure 7: Grain width trend with energy density (a) and cooling rate (b) (Mendoza et al. [2017])

The energy density is a critical manufacturing factor for the homogeneity and resultant properties of any AM deposition. There are other examples on how the energy density can determine not just the grain size, but also the porosity, lack of fusion and in some cases unmelted particles. Backscatter electron micrographs in Figure 8 show large field view of the xz plane of two different energy densities (high and low) depositions made using LENS$^{\mathbf{TM}}$ technology for a fixed composition of Ti-15Mo Mendoza et al. [2019]. By these two images, the sample with energy density of 7.4 MJ/in^3 (8b) shows less unmelted particles, less lack of fusion and a very high compositional homogeneity. On the other side, the sample with energy density of 2.4 MJ/in^3 (8a) shows a lack of fusion in almost all layers and in some cases as large as 500 μm. The unmelted particles of Mo are easy to visualize in the backscatter electron micrographs because the average atomic mass determines the contrast on those images. Therefore, the brighter regions are Mo rich zones and darker gray regions are rich in titanium.

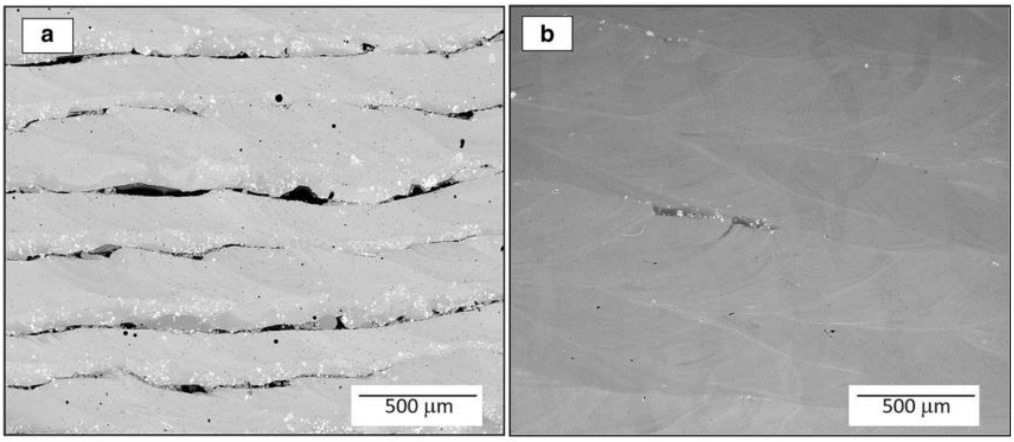

Figure 8: Micrographs of Ti-15Mo at 2.4 MJ/in^3 (a) and 7.4 MJ/in^3 (b) (Mendoza et al. [2019])

4.2 Residual stress

Dwell times between individual layer deposition is very common technique in additive manufacturing to allow additional colling time. The accumulation of residual stress in AM has several similarities with the welding process since both are a layer-by-layer deposition. In 1997, it was reported that reducing input energy leads to a lower workpiece distortion in welding Michaleris and DeBiccari [1997]. Later in 2003, it was reported that pre-heating the weld region can reduce the net distortion Deo and Michaleris [2003]. In a similar manner for additive manufacturing, preheating the bulk substrate can lead to a reduction of the residual stress and total distortion on the deposited material Jendrzejewski et al. [2004]. Additive manufacturing involves the deposition of multiple layers to build a component in larger dimensions compared to welding or laser cladding. Therefore, dwell times and path planning are important factors to determine the resultant residual stress and workpiece distortion. Decreasing dwell time between passes reduces the residual stress in deposited Co-based Stellite SF6 alloy Jendrzejewski and Śliwiński [2007]. Different position paths affect the residual stress and distortion in AISI 1117 C- Mn steel Nickel et al. [2001] and in AISI 316 austenitic stainless steel Mercelis and Kruth [2006].

In a more recent work in additive manufacturing, the dwell time and material selection were studied Denlinger et al. [2015]. In-situ measurements of temperature and distortion were performed in Ti-6Al-4V, and Ni-Cr-Mo solid solution strengthened Inconel$^{@}$625. This research work also compared one alloy with a solid-state allotropic transformation (Ti-6Al-4V) and another one that does not (Inconel$^{@}$625). Three different dwell times were used with the same input energy for both alloy systems Denlinger et al. [2015]. This study showed that increasing the dwell time to allow additional cooling time resulted in a reduction of residual stress in Inconel$^{@}$625. However, for the Ti-6Al-4V alloy, increasing the dwell time resulted in an augmented level of residual stress. Figure 9 shows the above-mentioned trend.

There are two main mechanism for the residual stress accumulation in additive manufacturing. The first mechanism is thermal stress due to the strong gradient of temperature between subsequent layers of deposition. These temperature gradients generate residual stress in the vertical direction predominantly. The second mechanism is the phase transformation due to solidification, and it has a preferential residual stress generation in the horizontal direction. In addition, additive manufactured Ti-6Al-4V at certain critical energy density value suffers a solid phase transformation. This transformation from β phase to a martensitic α' phase also induce residual stress on the deposited material Yakout et al. [2020].

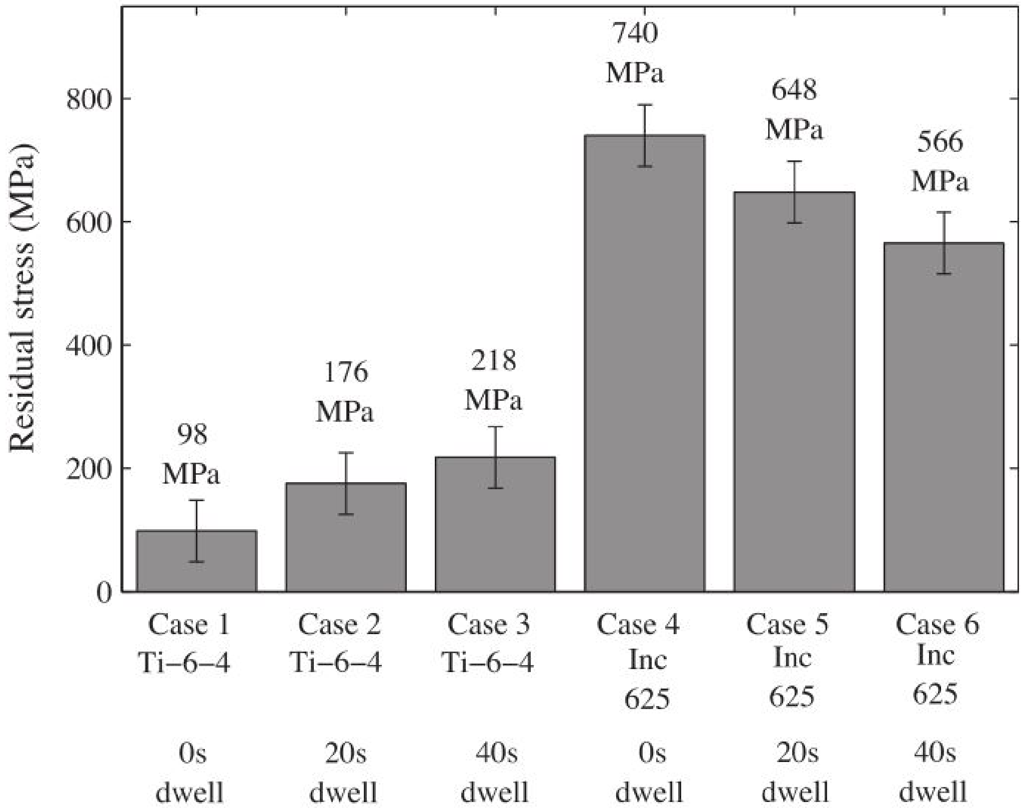

Figure 9: Variation of residual stress with dwell time for 6 cases (Denlinger et al. [2015])

In 2021, researchers worked on a study where the laser power and travel speed were fixed to evaluate the influence of laser scan strategies on residual stress. Four different strategies were used with 2 continues over the sample and the other 2 using small islands with alternating patterns Strantza et al. [2021]. They found very large residual stresses on the order of $1/2$ to $3/4$ of yield strength of additive manufactured Ti-6Al-4V with a concept laser equipment. The non-continuous or island strategies resulted in more residual stress specially at the extreme edges of the deposited material. On the other hand, a reduction of the residual stress was observed in the continuous scan strategy with a rotation of 90°C per layer. They suggest Strantza et al. [2021] that scan strategies allowing faster cooling rates are responsible for higher residual stress on deposited material. In addition, in the island strategy, those near to the edges show even faster colling rates producing even more residual stress.

4.3 Grain size, morphology, and texture

In additive manufacturing in general, the heat source melts the incoming material. For the LENS$^{\mathbf{TM}}$ specific case, the laser melts the powder metal creating a molten pool on a substrate. This molten pool experiences a very rapid colling of 104-106 K/s Strantza et al. [2021]. This unique condition leads to a unidirectional solidification of columnar grains (prior β grains for Ti-alloys). The substrate is acting as a strong heat sink promoting the vertical growth. Therefore, the columnar grains are a result of epitaxial growth from the bottom of the molten pool in direct contact with the substrate. Several examples of columnar grains are Ti-Mo system Mendoza et al. [2019] Ti-6Al-4V system Kelly and Kampe [2004] and Ti-Cr system Zhang et al. [2010]. Figure 10 shows an optical micrograph of a columnar morphology of a LENS^{TM} Ti-W sample.

Figure 10: Optical micrograph of Ti-6W alloy.

Equiaxed grains are also observed in AM deposited material. Normally, they develop at the top region of deposition. This phenomena occurs because the substrate acting as a heat sink at the bottom is less effective at the top. Unmelted particles at the top surface and the lower temperature gradient induce nucleation of new grains (Liu et al. [2021]). The columnar to equiaxed transition (CET) can also be achieved by a β annealing treatment after deposition (Zhu et al. [2015]) or adding alloying elements among others (S.Tamirisakandala et al. [2005]).

Regarding adding alloying elements to transform the morphology from columnar to equiaxed and reduce the grain size, there are many research publications about the topic. Many of them are focus on cast alloys and not in additive manufacturing. However, the factors affecting the grain size such as inoculants, cooling rates and compositional effects can be considered in AM. Recent work on grain refinement was considering the effect of the growth restriction factor as a thermodynamic parameter defining grain size. Equation 2 defines the growth restriction factor Q, where m is the slope of the liquidus line, c_0 is the solute concentration and k is the partition coefficient.

$$Q = mc_0(k-1) = \frac{d\Delta T_c}{df_s}. \tag{2}$$

The differential term to the right is expressing the concept of the growth restriction factor as the rate of development of constitutional supercooling (ΔT_c) relative to the rate of solid development (f_s). Boron (B) acting as a grain refiner was reported on Ti-6Al-4V and Ti-6242 (S.Tamirisakandala et al. [2005]). Similar studies applying the growth restriction factor of boron reported same results on as-cast commercially pure titanium (Bermingham et al. [2008]). The refiner power of boron was also noted in the review paper by Collins et al. analyzing the boron modified TNZT alloy (Collins et al. [2016]). The explanation for this phenomena is that boron solute is rejected in front of the solid-liquid interface. That boron rich region is undercooled and restricts the growth of any preexistent nuclei and promotes the activation of new nuclei.

Based on solute contributions and nuclei effects on grain size Easton & St. John developed a semi-empirical relationship to assess the grain refinement on Al and Mg alloys (Easton and St. John [2001]). The general relationship is expressed in Equation 3:

$$d = a + \frac{b}{Q}, \tag{3}$$

where d is grain diameter, a is the y-intercept defined in Equation 4, b is the slope defined in Equation 4 and Q is the already defined growth restriction factor:

$$a = \frac{1}{(\rho \cdot f)^{1/3}} \tag{4}$$

$$b = b_1 + \Delta T_n, \tag{5}$$

in Equation 4, ρ is the density of nucleant particles and f is the activated fraction of particles. This equation shows that a is inversely proportional to the maximum number of activated nuclei. For Equation 5, the term ΔT_n is the necessary undercooling to activate nucleation and b_1 is a constant. Therefore, the slope b basically represents the undercooling necessary to activate nucleation, higher values of b lead to lower potency of nuclei. Easton & St. John demonstrated the applicability of this concepts (equation) on Al and Mg alloys. However, ulterior studies (Banerjee et al. [2006]) demonstrated the extended applicability of the same concepts on Ti-alloys. All this work was based on as-cast Ti-alloys. Only in 2017, Mendoza et al. reported that despite the out of thermodynamical equilibrium condition of AM, it is possible to predict in some degree the grain refiner power of alloying elements by utilizing these concepts on additive manufacturing and more specifically of LENS$^{\mathbf{TM}}$ technology on titanium alloys (Mendoza et al. [2017]). Figure 11 shows three backscatter micrographs of average compositions of 5, 13 and 25 pct on the Ti-W system. The features in all micrographs are very similar with prior β grains with alpha laths inside the grains. However, the grain size was clearly reduced by the tungsten (W) additions (Mendoza et al. [2017]).

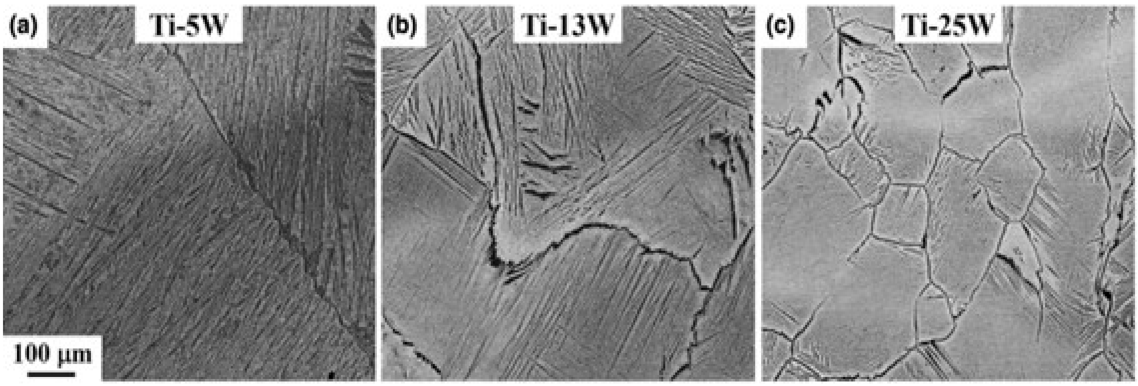

Figure 11: Backscatter micrographs of Ti-W system (Mendoza et al. [2017])

These results summarize the grain refiner power of tungsten as an alloying element with a high growth restriction factor of about 22.6 C_0. Later in 2019, same authors applied the same concept in AM with an alloying element with a very low growth restriction factor of 6.5C_0 (molybdenum). Figure 12 shows backscatter micrographs of a compositional gradient sample deposited with LENS$^{\mathbf{TM}}$ at locations of 0.9, 2.8 and 8.2 wt.% of Molybdenum (Mo). In this case, the prior

β grain size of the titanium alloy was not reduced by the Mo additions and the morphology was in fact columnar over the entire sample. These two higher (Ti-W) and lower (uTi-Mo) bound scenarios of grain refiners based on growth restriction factor sggest the applicability of the thermodynamical concepts on additive manufacturing.

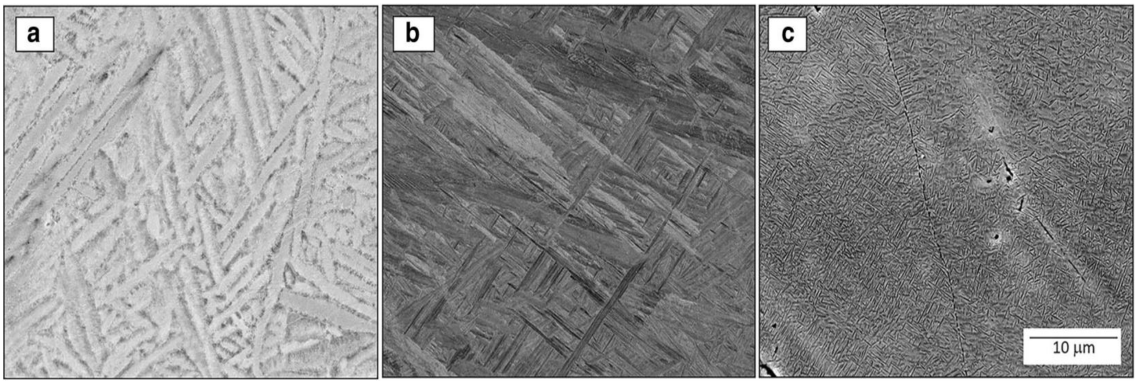

Figure 12: Backscatter micrographs of Ti-Mo System (Mendoza et al. [2019])

Tedman et al. worked with powder additions of W, Mo and Nb to assess their efficacy as nucleant particles in titanium alloys. The samples were deposited using wire arc additive manufacturing (WAAM), a technology that will be described in a further section in this chapter. They found that particles surviving the melting process are acting as potent nucleation points for β crystals. The alloying elements acting as inoculants suffer partial dissolution and enrich the surrounding liquid. That solute enrichment raised the equilibrium liquidus temperature and lead to preferential crystal growth or solidification upon the surface once the cooling process starts (Tedman-Jones et al. [2019]). They call that process as âdissolutional supercoolingâ which basically applies the same concept of constitutional undercooling at the solidification front analyzed previously in the Ti-W system (Mendoza et al. [2019]). They call that process as âdissolutional supercoolingâ which basically applies the same concept of constitutional undercooling at the solidification front analyzed previously in the Ti-W system (Mendoza et al. [2019]). Other efforts were focus on evaluating grain size and morphology for three different Ti-alloy systems. The idea was to compare non-growth restricting solutes or nucleant particles in a Ti-6Al-4V alloy, containing growth restricting solutes, but non-nucleant particles in a Ti-3Al-8V-6Cr-4Mo-4Zr alloy and the last system was containing all the previous growth restricting solutes and including nucleant particles in a Ti-3Al-8V-6Cr-4Mo-4Zr + La_2O_3. The results on first system were large grain size and a combination of columnar and equiaxed grain morphology. The second system refined the grain size by 55% but did not show a significant columnar to equiaxed transition (CET). However, the last system with the La_2O_3 additions (nucleant particles) refined the grain size over 85% and produced a clear zone of equiaxed grains at the top of each layer (Bermingham et al. [2019]).

In 2022, efforts to improve the understanding of solute and nucleant particles were focus on aluminum alloys, but using alloying elements as Si, Cu and Ni (Tan et al. [2022]). They concluded that despite the rapid solidification in AM, a high enough solute concentration is still necessary to create the constitutional undercooling which in turn induce heterogenous nucleation (grain refinement). In addition, it was demonstrated that additions of strong nucleant particles as lanthanum hexaboride (LaB6) (Tan et al. [2022]) and high melting point yttria (Y_2O_3) particles (Wang et al. [2021]) highly increases th$_2$e grain refinement in their AM depositions.

Regarding texture, there is a large number of researchers reporting the <001> texture which is concordant with the greatest temperature gradient in the vertical direction (z axis). Ni based alloy IN738LC made by selective laser melting shows the characteristic <001> texture (Kunze et al.

[2015]). It is also the case for Ti-alloys (Qiu et al. [2015]). However, additions of Zn, Mg and Ti in cubic systems as Al-alloys can deviate the <001> texture to be <110> (Collins et al. [2016]). In a more recent approach for an additive manufactured Ti-6Al-4V study, it was demonstrated that the scanning strategy can modify texture and microstructure (Quintana et al. [2020]). This phenomena could be related to different thermal cycles allowing different cooling rates affecting solidification and texture.

5 Electron Beam Additive Manufacturing (EBAM@)

Electron beam additive manufacturing technique is a metal 3D printing process launched by Sciaky Inc. in 2009. The system uses an electron beam as the heat source and a wire is fed into the electron beam to create the molten pool in a vacuum chamber. The vacuum chamber is a requirement for the electron beam and also provides a non-reactive environment for the deposition of high purity materials (Mendoza Londono [2016]). In general, wire feed systems as EBAM@ are suitable for large-scale volumes due to its high deposition rates (Frazier [2014]). This technique can produce high quality structures, up to 19 inches length, made of Titanium, Nickel-based alloys, and tantalum among others in days (Inc [2022]). The original purpose to develop EBAM@ was for aerospace applications. However, it is now beneficial for a wide range of industries and applications where reducing cost and time is top priority. Some examples of EBAM@ applications are Oil & gas equipment, turbine blades for energy production, medical equipment, industrial pump components and marine propulsion. Figure 13 shows a schematic view of the EBAM@ technology. A unique advantage of EBAM@ is the dual wire feed system that allows to combine two different metals or alloys to create a specific custom alloy. In addition, it is also possible to change the mixture ratio of the wire feed to create a graded part as in LENS™. After the part is completed, a heat treatment, machining and final inspection is performed. (Inc [2022]).

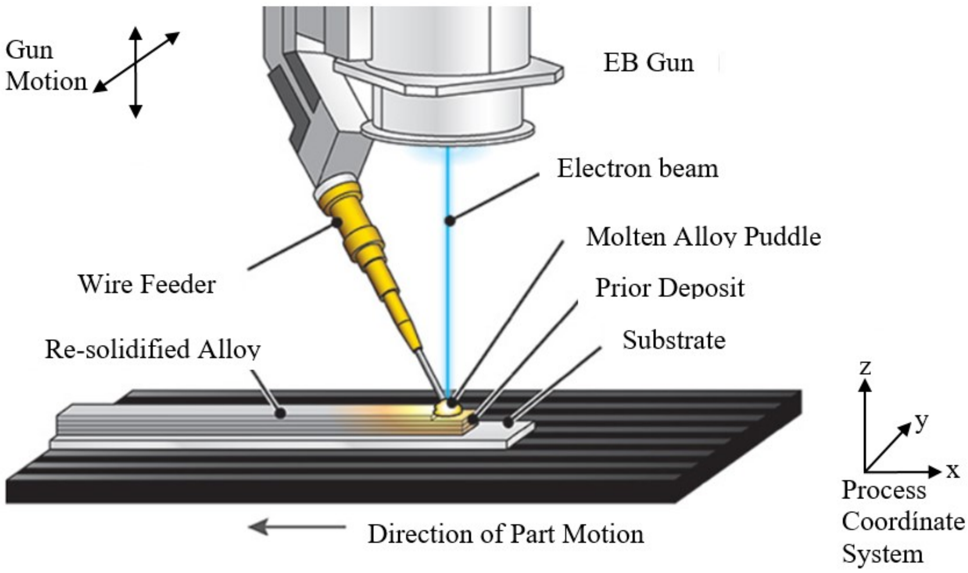

Figure 13: Schematic view of the EBAM@ technology (Inc [2022])

Discontinuities in EBAM@ are similar as in LENS™ including porosity and lack of fusion between layers. However, porosity is less, and unmelted particles are not present because EBAM@ does not operate with powder. Wire systems have higher deposition rates which represents deposition of larger objects that are ideal for large mechanical systems as air frame structures or aircraft engines. It can be equipped with multiple nozzles with different metals in a single electron beam gun to create custom alloys.

Regarding the residual stress in electron beam additive manufacturing, it is governed by temperature gradients and phase transformations during solidification as described in section 4.2. In EBAM@, the deposition rate is higher compared with LENS**TM** which leads to lower dwell time. The direct implication of less time between layers was described as material dependent as illustrated in Figure 9 comparing Ti-6Al-4V with Inconel@625 in section 4.2. Grain size, morphology and texture is equivalent to the described in section 4.3 for LENS**TM**, but due to the larger scale volume and speed of deposited material, it needs to consider different thermal cycles. Hayes et al. shows a good example of microstructure features under EBAM@ (Hayes et al. [2017]).

In general, both technologies are applying the same principles with small differences that can affect the resultant properties of the deposited material. It is important to mention that on average, AM-Grade Ti-6Al-4V powder is 141% more expensive than the AM-Grade Ti-6Al-4V wire. The use of metallic powder also represents a higher safety concern because breathing in fine particles, such as titanium or nickel, can be harmful (Inc [2022]).

6 Wire Arc Additive Manufacturing (WAAM) and Marine Applications

As described in section 1, titanium and its alloys are used due to their excellent corrosion resistance in aerospace, chemical and power plants among other industries, but it is generally used little to build ships. In 2002, Nippon Steel corporation completed all-titanium ships in cooperation with shipbuilders (Kimura et al. [2002]). The critical question is how additive manufacturing and specifically titanium alloys can contribute to marine or naval applications. The industrial marine environment is dominated by complex and ever larger components when compared with other industries (e.g., aerospace industry). It is also a harsh and corrosive environment for systems such as offshore platforms and various ship classes (Strickland [2016]). Wire arc additive manufacturing (WAAM) is another AM technique with additional capabilities to manufacture large-scale components. WAAM has a much higher deposition rate than other AM techniques (e.g., LENS**TM** and EBAM@) making it suitable for marine applications (Wang et al. [2012]). In this section, wire arc additive manufacturing technique is described with an emphasize in marine applications.

6.1 Wire arc additive manufacturing

This is a metallic 3D printing machine, where metallic wires are the feeding material, and the heat source is an electric arc. The protective environment depends on the type of arc welding. The original idea of WAAM was in 1925 with a simple arc welding to deposit ornaments (Ralph [1925]). After about one century of development, WAAM becomes suitable for new applications. In this process a wire is fed into an electric arc and melted with the substrate or the previous deposited layer. The efficiency of the material is near to the 100% because there is not powder handling and not unmelted particles. The cost associated with WAAM is around one order of magnitude less when compared with laser-based powder processes. Discontinuities in WAAM are basically the same as those in EBAM@), considering that both techniques are using a wire feedstock. The high deposition rate of WAAM allows the manufacture of very large-scale components. However, some drawbacks such as low density due to violent melt pool interaction, poor surface quality and less dimensional accuracy (Rosli et al. [2019]). Figure 14 shows a WAAM system integrated with a MIG/MAG at the welding institute (TWI). In addition, due to the size and speed of depositions the dwell time is less between layers, and it has been reported with different effects on residual stress depending on material (section 4.2). However, due to the large heat source, a high tensile residual stress might be induced (Lin et al. [2021]). The WAAM systems can be divided into three main systems and a fourth one designed for titanium alloys. In general, they are based in traditional welding methods such as gas metal arc welding (GMAW), gas tungsten arc welding (GTAW) and plasma arc welding (PAW). Robotic welding systems are the based to integrate these three simple configurations (Lin et al. [2021]). The selection of material and welding technology are driven by the user application. For instance, if quality and process stability are a priority, GTAW should be preferred over GMAW. On the other hand, GMAW is preferred if the priority is high deposition rate (Cunningham et al. [2018]). However, the PAW system offers good quality and high deposition rate, but with higher initial cost. Several metals and alloys have been used for WAAM process such as steels, stainless steel, nickel-based alloys, aluminum alloys and titanium alloys. The last alloys system has superior properties (Lin et al. [2021]) and is the focus of attention for metals in additive manufacturing in different industries such as aerospace, military and weapons, marine and shipbuilding. However due to the high cost of titanium, the applicability is limited in several industries.

6.1.1 GMAW based WAAM system

Gas metal arc welding is a welding process where an electric arc is created between the substrate (workpiece metal) and the electrode (consumable wire). The wire is fed continuously and melted in a molten pool protected by a shielding gas (e.g., argon helium etc.). The Figure 15 shows the configuration of the GMAW-WAAM integrated system. The current and voltage are the key parameters to control the GMAW-WAAM system because it controls the input energy. Due to the nature of the heat source high thermal inputs are received by the wire and substrate. This leads to unwanted deformations resulting in dimensional tolerances of ± 1 mm (Prado-Cerqueira et al. [2017]). In order to remove the non-suitable surface finish, the company FRONIUS GmbH patented the cold metal transfer technique (CMT) (Office) [2022]). In CMT, the current intensity and voltage are controlled to transfer metal to the molten pool and retracting the electrode at very short intervals to produce a clean, splatter-free deposition. The process integrates the movement and deposition of material in four phases described in detail by (Prado-Cerqueira et al. [2017]).

6.1.2 GTAW based WAAM system

Gas tungsten arc welding is a process where a non-consumable tungsten electrode provides the heat, and an independent wire is fed to produce the deposited material in the molten pool. In this technique the wire feed orientation has a strong influence on the transfer material and quality of the deposit. Front, back and side feeding are normally used, but front feeding is the regular orientation for Ti-alloys and Fe-Alloys (Shen et al. [2016]). Figure 16 shows the configuration of GTAW-WAAM system. This configuration has a gas lens to guarantee the shielding gas is in laminar flow to reduce oxidation. It is very important for titanium alloys due to the high reactivity with oxygen at high temperatures. Normally, a tracing shielding device is used to protect titanium alloys and that will be discussed in a subsequent section (Pan et al. [2018]).

GTAW-WAAM has the capability to manufacture compositionally graded materials as with (LENS$^{\mathbf{TM}}$) or (EBAM$^{@}$) technologies (Shen et al. [2016]). For this objective, two different wire-feed systems can provide different metals or alloys to the molten pool. The deposited material composition can be controlled by adjusting the wire-feed rate independently just as in blown powder systems. Preheating the substrate and placing suitable tracing shielding help to control the interlayer temperature and reduce oxidation, especially critical for titanium alloys (Pan et al. [2018]).

Figure 14: WAAM system used at TMI (Office) [2022])

6.1.3 PAW based WAAM system

Plasma arc welding is a process where a plasma is used to transfer an electric arc to a work piece or parent material. Then the metal to be welded is melted by the intense heat generated by the electric arc. Plasma is defined as a gas that was heated to a very high temperature and ionized to make it electrically conductive (Mannion and Heinzman [1999]). The torch in PAW has a tungsten electrode with a copper nozzle for the plasma. They create a pilot arc that is transferred to the metal to be welded. The arc energy in plasma welding can reach three times the GTAW (Pan et al. [2018]).

Plasma gases are usually argon, and the torch system has also a secondary gas source that can be helium, hydrogen, and argon to play the shielding role. The distance from workpiece to the

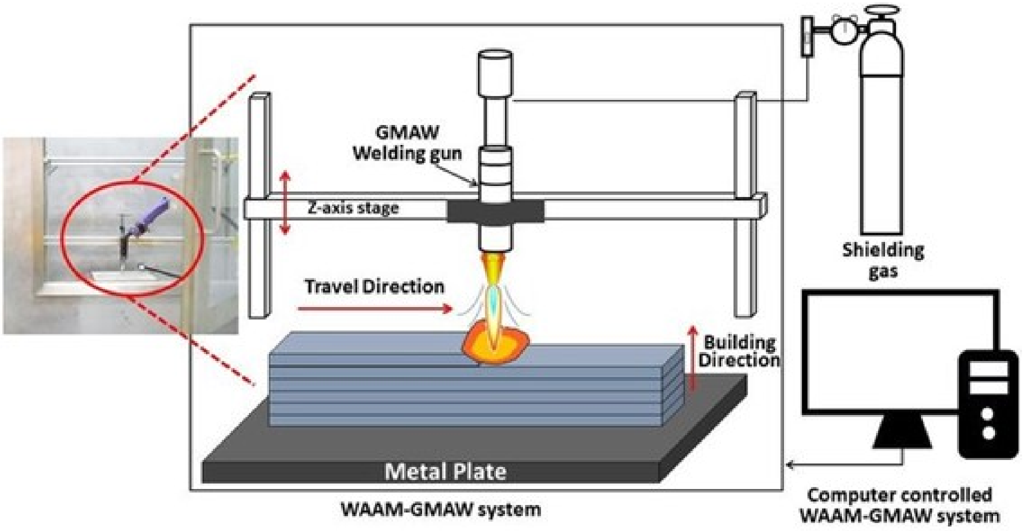

Figure 15: Schematic GMAW-WAAM integrated system (Rosli et al. [2019])

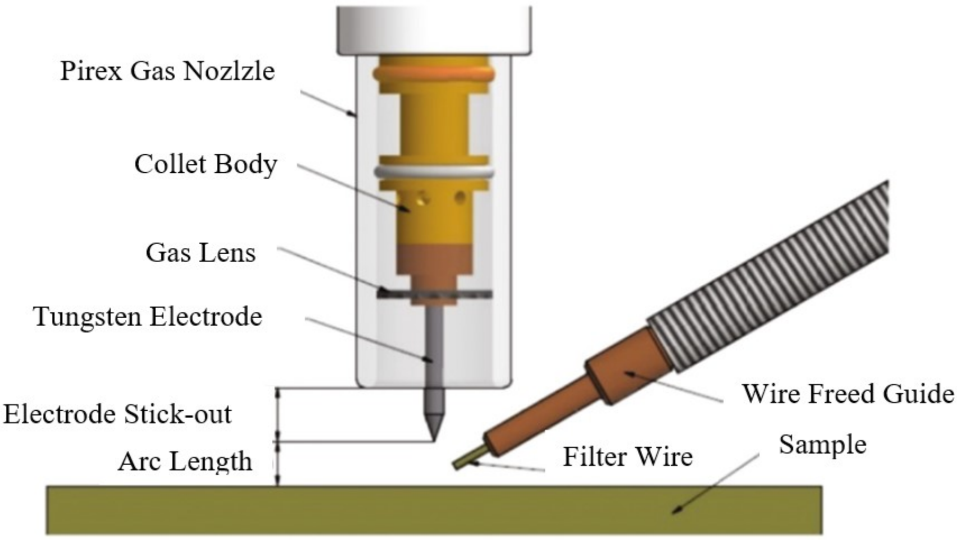

Figure 16: Schematic GTAW-WAAM integrated system (Pan et al. [2018])

tungsten electrode tip (stand-off distance) is not as critical as in GTAW due to the cylindrical and focus arc shape of PAW (Mannion and Heinzman [1999]). Therefore, the arc transfer is gentle and consistent to produce high quality deposits of material. The stability of the electric arc reduces the arc wander effect which is a deflection of the arc that can lead to lack of fusion imperfections (Mannion and Heinzman [1999]). The Table 2 shows a basic comparison of these three WAAM systems.

6.2 WAAM systems to manufacture titanium-alloy components

As mentioned in section 6.1.2 Titanium and its alloys are very reactive with oxygen at elevated temperatures. Several researchers reported severe oxidation on WAAM Ti-based components (Bermingham et al. [2018]). That reactivity produces oxides that embrittle the deposited mate-

Table 2: Comparison of WAAM systems (Lin et al. [2021])

WAAM systems	Deposition rate (kg/h)	Stability	Cost	Heat input	Thermal efficiency
GMAW-based	3-4	Splash	Low	High	84%
GTAW-based	1-2	Good	Low	Low	67%
PAW-based	2-4	Good	High	High	47%

rial, making the WAAM system not very suitable for Titanium alloys. To prevent oxidation on titanium some researchers have been used a closed chamber filled with inner gas (Alonso et al. [2019]). However, the chamber adds several limitations to the manufacturing process. First, the chamber restricts the size of the components to be smaller than the chamber itself. The robot arm movement is also restricted which affects the direction and rate of deposition. Therefore, the use of chambers to manufacture titanium alloys is not very practical for large-scale or ultra-large-scale parts as required for the naval industry (Lin et al. [2021]).

To eliminate the closed chamber requirement several efforts, propose the use of tracing shielding devices (Lin et al. [2021]). This device is usually fixed to the torch and provides a focalized distribution of inert gas to cover only the latest deposited region to prevent the oxidation. Figure 17 shows trace shielding designs for the basic WAAM systems. The tracing shielding device has been a custom-made feature added only to fit specifical needs in a particular application.

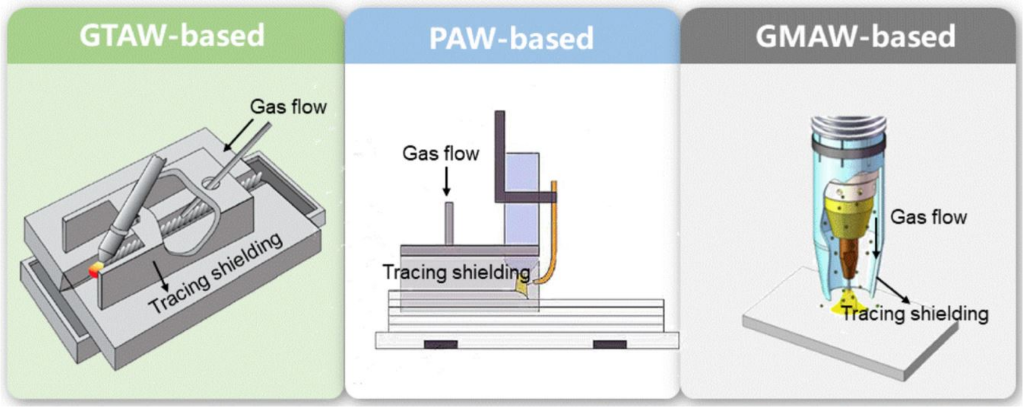

Figure 17: Tracing shielding design for WAAM (Lin et al. [2021])

The grains size as described in section 4.3 with (LENS^{TM}) deposits is governed by epitaxial growth which is inherent to any AM technique. In this case, several hybrid WAAM systems have been designed to promote grain refinement on titanium alloy deposits (Lin et al. [2021]). Martina et al. proposed one of those hybrid-WAAM systems with a preheating of deposited layer during the deposition of the next layer. This modification resulted in a good refinement of the prior β grains and a columnar to equiaxed transition (CET). This custom-adapted process is named inter-pass rolling (IRWAAM) (Martina et al. [2015]).

6.3 Naval and Offshore applications

Titanium is considered an optimal material for the excellent corrosion resistance in sea water. However, due to cost and other manufacturing considerations it is not widely used in the naval and offshore industry. During more than 50 years offshore steel structures were designed with corrosion allowance and not considering for a real corrosion protection (Kimura et al. [2002]). In 1997, the only corrosion allowance idea is abandoned and new methods to offer certain degree of corrosion protection are proposed. The titanium-clad steel covering on the piers (splash and tidal zones) of the Trans-Tokyo Bay (TTB) (i.e., Aqua-Line) was one of the first corrosion protection methods implemented on offshore infrastructure (Kimura et al. [2002]). Covering existing steel pipe piles with 0.5 mm thick titanium sheet has been a work performed for many years at Nippon Steel Nagoya works. Shipyards in Japan use titanium to manufacture several parts such as exhaust cooling pipes, mufflers, fire-fighting sea water guide pipes and valves, ladders, shafts and propellers due to corrosion resistance or weight reduction (Kimura et al. [2002]).

The naval industry is characterized by a very specific operating conditions of equipment and machinery. For instance, ships have unique operational requirements of reliability and safety. The original equipment manufacturer or local authorities imposed quantity and type of spare parts to be on board (Kostidi and Nikitakos [2018]) for safety reasons. Spare parts inventory is necessary to avoid or reduce breakdowns or ship downtime. If a damage in the ship appears, the spare part needs to be used to continue normal operation. However, if the spare part is not in stock, a request needs to be sent to the land office. From this perspective additive manufacturing could be used on board to manufacture spare parts on demand, reducing the spare part inventory and consequently the cost.

In 2015, the container shipping company MAERSK reported the installation of 3D printers (AM) on board to fabricate spare parts (Kostidi and Nikitakos [2018]). In addition, the US navy has implemented the installation of 3D printers (AM) for afloat manufacturing of spare parts (Strickland [2016]). The benefits from this approach can improve operational efficiency in areas of spare parts and tooling. However, there are some technical concerns regarding the static environment that those AM techniques require for quality of deposited or printed material (Strickland [2016], Kostidi et al. [2021]).

Queguineur et al. made an evaluation of wire arc additive manufacturing (WAAM) on large-scale components for naval applications (Queguineur et al. [2018]). Their objective was to study the processing parameters optimization associated with the mechanical properties of stainless steel (AISI 316L) and copper-aluminum alloy (Cu-8Al-2Ni-2Fe) with a GMAW-WAAM system. They demonstrated that GMAW-WAAM technology is an alternative to cast products for the naval industry in terms of mechanical and corrosion results for the AISI 316L. The Cu-Al alloys showed a slight decrease in mechanical behavior compared with as cast products (Queguineur et al. [2018]). However, this result only represents that further research needs to be addressed to better implement AM technology in naval applications.

The current use of additive manufacturing or 3D printing in the naval industry, is limited to auxiliary components for ships. Those components or spare parts are engines, heat exchangers, valves, pumps and propellers (BAYRAMOÄLU et al. [2019]). In Netherlands, the association of RAMLAB, Promarin, Autodesk, Bureau Veritas and Damen shipyard manufactured the worldâs first-class 3D-printed ship propeller, named as WAAMpeller. Figure 18 shows the successful implemented WAAMpeller by RAMLAB. The WAAMpeller has a diameter of 1.3 m, weight of 180 kg and was manufactured to drive a Stan Tug 1606 (Ziółkowski and Dyl [2020]. The whole manufacturing process was supervised and certified by Bureau Veritas. The used material was an aluminum, nickel, and bronze alloy.

A recent effort on AM propeller was reported to use a numerical approach to design a hollow blade that was also fabricated to correlate the optimization process (Muller et al. [2019][2019]). The process of producing a hollow blade is very difficult to conventional foundry process and offers the option to control thickness in different sections of the hollow blade (See Figure 19). This concept could lead to a reduction of initial raw material and an augmented hydrodynamic performance compared with solid propellers (Muller et al. [2019][2019]).

The study reported an improvement of the hydrodynamic performance by reducing cavitation and mass reduction of 23% in air and 36% in water (Muller et al. [2019] [2019]). Other benefits presented were the reduction of underwater radiated noise at higher frequencies where cavitation

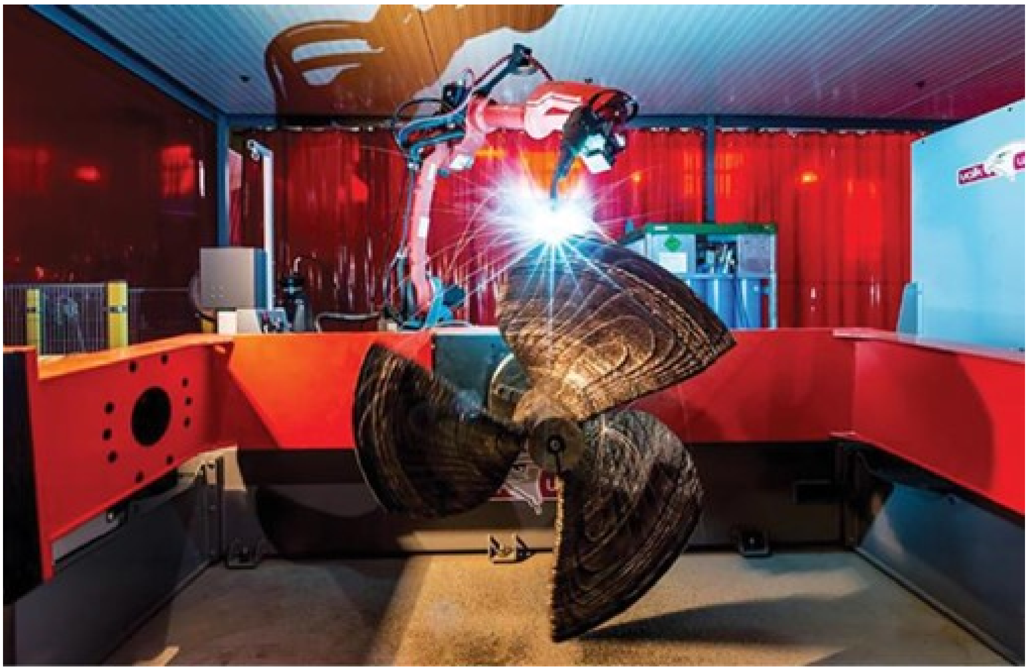

Figure 18: WAAMpeller (BAYRAMOÄLU et al. [2019])

Figure 19: Hollow blade (Muller et al. [2019] [2019])

is the main contributor. In the offshore industry, marine risers are often subjected to structural and functional requirements. The failure of those components can imply severe environmental and economic impacts. Marine risers are subjected to corrosion attack due to hydrogen sulphide, Chlorides, and carbon di-oxide gases. At the same time, they are also under continuous environmental loads; wind, waves, current, ice, and impacts. Because of the above, the innovation in conventional design of the marine risers is a challenge because of the increase of the water depth on offshore production, especially in sensitive zones as the weld on the thick forged ends, counter-bored riser pipe, and cladding along with the critical locations, e.g. of susceptible zones can be observed in Figure 20.

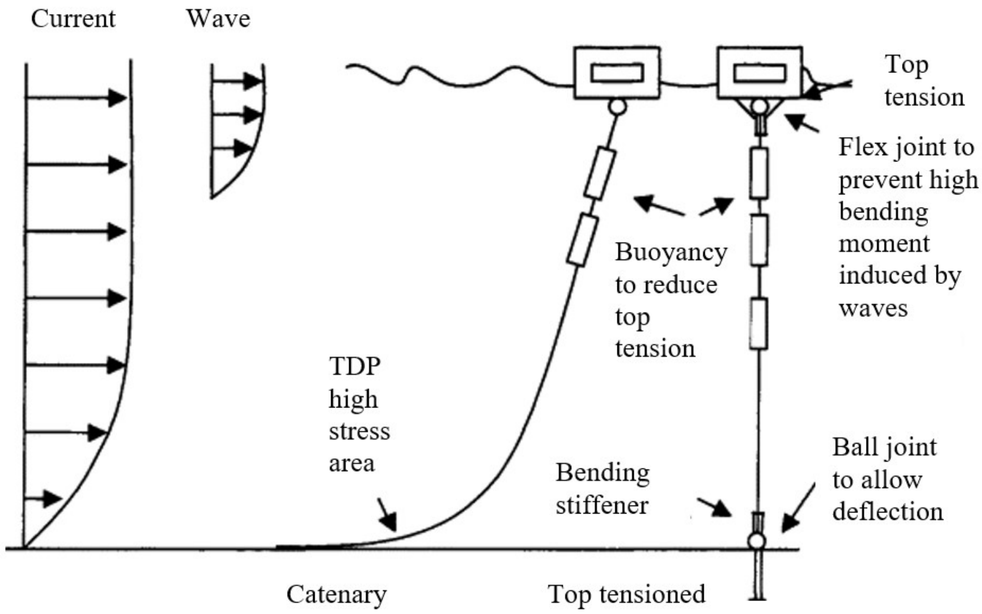

Figure 20: Example of tensions of risers at top and bottom, and external enviromental loads(Bai and Bai [2005])

Among those, the risers in some cases must withstand pressures over 20,000 psi (137,89 MPa) and temperatures exceeding 176°C. Sandwich composite risers can be an alternative to those challenges, but delamination can be a threat to their use under the combination of thermal and mechanical loads. Under high temperature and pressure effects (HTHP) thermal stresses occur at the metal and ceramics bonding interface due the differences of their thermal expansion, this can lead to a crack formation and delamination in the interface. Functionality Graded Materials (FGM) are designed to overcome this damages because they possess no distinct material interfaces. FGM′s are produced by several AM techniques, the WAAM technique was used in the work of Chandrasekaran et al. [2022], where a test specimen was produced composed by Duplex stainless steel and Carbon Manganese Steel as can be observed in Figure 21.

This composition is chosen based on the functional requirements without compromising the strength criteria. Tension test, and X-Ray computed Tomography analysis where performed. The X-Ray Computed Tomography showed that the WAAM process is acceptable for part fabrication. From the mechanical properties, it is seen that the yield and ultimate strengths of FGM are higher by 11.16% and 24.75%, respectively, in comparison with that of the standard X52 steel used in marine risers. The toughness, strength ratio, and ductility ratio are also higher for the FGM samples, while Modulus of Elasticity and Poisson′s ratio values are in the same range as X52 steel. Other potential application is the case of offshore wind applications, where the same benefits of WAAM technique can be applied to overcome monopile residual stress derived from corrosion-fatigue, improving by this technique the fatigue life (Ermakova et al. [2019]).

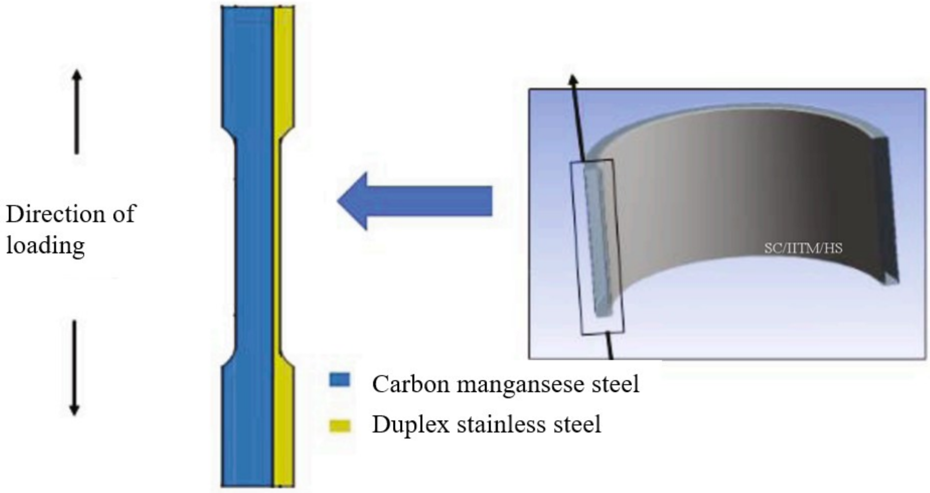

Figure 21: Sectional view showing the region where the mechanical properties are determined (along the longitudinal axis of the FGM marine riser), Chandrasekaran et al. [2022]

7 Concluding Remarks

Additive manufacturing techniques (i.e., 3D printing) are growing in different industries. However, the Naval and Offshore industry is characterized as conservative to changes and the major development of AM has been in the aerospace and automotive sectors. The knowledge generated by those sectors and the most recent implementation of that technology in the naval and offshore industry can reveal the benefits and challenges. WAAM and titanium alloys for the those industry is still a new topic and there are several technical challenges such as oxidation protection, distortion control and static environment. Regarding ship propellers and offshore systems such as risers and offshore wind platforms there is a wide opportunity to explore materials and design in WAAM systems to reduce cost and improve hydrodynamic and mechanical performance.

Acknowledgements

The authors gratefully acknowledge the Faculty of Sciences of Engineering - Universidad Austral de Chile for their support and encouragement for this publication.

References

U. Alonso, F. Veiga, A. Suárez, and T. Artaza. Experimental investigation of the influence of wire arc additive manufacturing on the machinability of titanium parts. *Metals*, 10(1):24, 2019. ISSN 2075-4701.

H. Attar, M. Calin, L. C. Zhang, S. Scudino, and J. Eckert. Manufacture by selective laser melting and mechanical behavior of commercially pure titanium. *Materials Science and Engineering: A*, 593:170–177, 2014. ISSN 09215093. doi: 10.1016/j.msea.2013.11.038.

Y. Bai and Q. Bai. Chapter 22 - Design of Deepwater Risers. In Y. Bai and Q. Bai, editors, *Subsea Pipelines and Risers*, chapter 22, pages 401–412. Elsevier Ltd., elsevier s edition, 2005. ISBN

9780080445663,. doi: https://doi.org/10.1016/B978-008044566-3.50024-5. URL https://www.sciencedirect.com/science/article/pii/B9780080445663500245.

R. Banerjee, S. Nag, S. Samuel, and H. L. Fraser. Laser-deposited Ti-Nb-Zr-Ta orthopedic alloys. *J Biomed Mater Res A*, 78(2):298–305, 2006. ISSN 1549-3296 (Print) 1549-3296 (Linking). doi: 10.1002/jbm.a.30694. URL http://www.ncbi.nlm.nih.gov/pubmed/16637044.

K. BAYRAMOÄLU, K. D. KAYA, S. YILMAZ, B. GÖKSU, and B. MURATO. Utilization of 3D Printing Technologies in Marine Applications. In *4th International Congress on 3D Printing (Additive Manufacturing) Technologies and Digital Industry*, 2019.

M. J. Bermingham, S. D. McDonald, K. Nogita, D. H. St. John, and M. S. Dargusch. Effects of boron on microstructure in cast titanium alloys. *Scr. Mater.*, 59(5):538–541, 2008. ISSN 13596462. doi: 10.1016/j.scriptamat.2008.05.002.

M. J. Bermingham, S. D. McDonald, D. H. StJohn, and M. S. Dargusch. Beryllium as a grain refiner in titanium alloys. *J. Alloys Compd.*, 481(1-2):L20–L23, 2009. ISSN 09258388. doi: 10.1016/j.jallcom.2009.03.016.

M. J. Bermingham, J. Thomson-Larkins, D. H. St John, and M. S. Dargusch. Sensitivity of Ti-6Al-4V components to oxidation during out of chamber Wire+ Arc Additive Manufacturing. *Journal of Materials Processing Technology*, 258:29–37, 2018. ISSN 0924-0136.

M. J. Bermingham, D. H. StJohn, J. Krynen, S. Tedman-Jones, and M. S. Dargusch. Promoting the columnar to equiaxed transition and grain refinement of titanium alloys during additive manufacturing. *Acta Materialia*, 168:261–274, 2019. ISSN 1359-6454.

S. Chandrasekaran, S. Hari, and M. Amirthalingam. Functionally graded materials for marine risers by additive manufacturing for high-temperature applications: Experimental investigations. *Structures*, 35(December 2021):931–938, 2022. ISSN 23520124. doi: 10.1016/j.istruc.2021.12.004. URL https://doi.org/10.1016/j.istruc.2021.12.004.

L.-Y. Chen, Y.-W. Cui, and L.-C. Zhang. Recent development in beta titanium alloys for biomedical applications. *Metals*, 10(9):1139, 2020.

P. Collins. The influence of the enthalpy of mixing during the laser deposition of complex titanium alloys using elemental blends. *Scr. Mater.*, 48(10):1445–1450, 2003. ISSN 13596462. doi: 10.1016/s1359-6462(03)00081-2.

P. C. Collins, D. A. Brice, P. Samimi, I. Ghamarian, and H. L. Fraser. Microstructural Control of Additively Manufactured Metallic Materials. *Annu. Rev. Mater. Res.*, 46(1):63–91, 2016. ISSN 1531-7331 1545-4118. doi: 10.1146/annurev-matsci-070115-031816.

M. Courtois, M. Carin, P. Le Masson, S. Gaied, and M. Balabane. A complete model of keyhole and melt pool dynamics to analyze instabilities and collapse during laser welding. *Journal of Laser Applications*, 26(4):42001, 2014. ISSN 1938-1387. doi: 10.2351/1.4886835.

C. R. Cunningham, J. M. Flynn, A. Shokrani, V. Dhokia, and S. T. Newman. Invited review article: Strategies and processes for high quality wire arc additive manufacturing. *Additive Manufacturing*, 22:672–686, 2018. ISSN 2214-8604.

E. R. Denlinger, J. C. Heigel, P. Michaleris, and T. A. Palmer. Effect of inter-layer dwell time on distortion and residual stress in additive manufacturing of titanium and nickel alloys. *Journal of Materials Processing Technology*, 215:123–131, 2015. ISSN 0924-0136.

M. Deo and P. Michaleris. Mitigation of welding induced buckling distortion using transient thermal tensioning. *Science and technology of Welding and Joining*, 8(1):49–54, 2003. ISSN 1362-1718.

M. Easton and D. H. St. John. A Model of Grain Refinement Incorporation Alloy Constitution and Potency of Heterogeneous Nucleant Particles. *Acta Mater.*, 49:1867–1878, 2001.

A. Ermakova, A. Mehmanparast, and S. Ganguly. A review of present status and challenges of using additive manufacturing technology for offshore wind applications. *Procedia Structural Integrity*, 17:29–36, 2019. ISSN 24523216. doi: 10.1016/j.prostr.2019.08.005. URL `https://doi.org/10.1016/j.prostr.2019.08.005`.

W. E. Frazier. Metal Additive Manufacturing: A Review. *J. Mater. Eng. Perform.*, 23(6):1917–1928, 2014. ISSN 1059-9495 1544-1024. doi: 10.1007/s11665-014-0958-z.

X. Gong, S. Mohan, M. Mendoza, A. Gray, P. Collins, and S. R. Kalidindi. High Throughput Assays for Additively Manufactured Ti-Ni Alloys Based on Compositional Gradients and Spherical Indentation. *Integrating Materials and Manufacturing Innovation*, 2017. ISSN 2193-9772. doi: 10.1007/s40192-017-0100-9. URL `https://doi.org/10.1007/s40192-017-0100-9`.

D. D. Gu, W. Meiners, K. Wissenbach, and R. Poprawe. Laser additive manufacturing of metallic components: materials, processes and mechanisms. *International Materials Reviews*, 57(3): 133–164, 2013. ISSN 0950-6608 1743-2804. doi: 10.1179/1743280411y.0000000014.

B. J. Hayes, B. W. Martin, B. Welk, S. J. Kuhr, T. K. Ales, D. A. Brice, I. Ghamarian, A. H. Baker, C. V. Haden, D. G. Harlow, H. L. Fraser, and P. C. Collins. Predicting tensile properties of Ti-6Al-4V produced via directed energy deposition. *Acta Materialia*, 133:120–133, 2017. ISSN 13596454. doi: 10.1016/j.actamat.2017.05.025.

N. Hrabe and T. Quinn. Effects of processing on microstructure and mechanical properties of a titanium alloy (Tiâ6Alâ4V) fabricated using electron beam melting (EBM), part 1: Distance from build plate and part size. *Mater. Sci. Eng*, 573:264–270, 2013.

S. Inc. Make Metal Parts Faster Cheaper with EBAM® Metal 3D Printing Technology., 2022. URL `https://www.sciaky.com/additive-manufacturing/electron-beam-additive-manufacturing-technology`.

R. Jendrzejewski and G. Śliwiński. Investigation of temperature and stress fields in laser cladded coatings. *Applied Surface Science*, 254(4):921–925, 2007. ISSN 0169-4332.

R. Jendrzejewski, G. Śliwiński, M. Krawczuk, and W. Ostachowicz. Temperature and stress fields induced during laser cladding. *Computers structures*, 82(7-8):653–658, 2004. ISSN 0045-7949.

S. M. Kelly and S. L. Kampe. Microstructural evolution in laser-deposited multilayer Ti-6Al-4V builds: Part I. Microstructural characterization. *Metallurgical and Materials Transactions*, 35 (6):1861, 2004. ISSN 1073-5623.

K. Kimura, K. Kinoshita, K. Tokuno, and H. Shimizu. Application of titanium to construction, civil engineering and ocean development. *Nippon Steel Technical Report*, pages 6–10, 2002. ISSN 0300-306X.

P. A. Kobryn, E. H. Moore, and S. L. Semiatin. The effect of laser power and traverse speed on microstructure, porosity, and build height in laser-deposited Ti-6Al-4V. *Scripta Materialia*, 43 (4):299–305, 2000. ISSN 1359-6462.

E. Kostidi and N. Nikitakos. Is it time for the maritime industry to embrace 3d printed spare parts? *TransNav: International Journal on Marine Navigation and Safety of Sea Transportation*, 12 (3), 2018. ISSN 2083-6473.

E. Kostidi, N. Nikitakos, and I. Progoulakis. Additive Manufacturing and Maritime Spare Parts: Benefits and Obstacles for the End-Users. *Journal of Marine Science and Engineering*, 9(8): 895, 2021.

D. A. Kriczky, J. Irwin, E. W. Reutzel, P. Michaleris, A. R. Nassar, and J. Craig. 3D spatial reconstruction of thermal characteristics in directed energy deposition through optical thermal imaging. *Journal of Materials Processing Technology*, 221:172–186, 2015. ISSN 09240136. doi: 10.1016/j.jmatprotec.2015.02.021.

K. Kunze, T. Etter, and J. Grässlin. Texture, anisotropy in microstructure and mechanical properties of IN738LC alloy processed by selective laser melting (SLM). *Mater. Sci. Eng. A*, 620: 213–222, 2015.

Z. Lin, K. Song, and X. Yu. A review on wire and arc additive manufacturing of titanium alloy. *Journal of Manufacturing Processes*, 70:24–45, 2021. ISSN 1526-6125.

Z. Liu, B. He, T. Lyu, and Y. Zou. A Review on Additive manufacturing of titanium alloys for aerospace applications: directed energy deposition and beyond Ti-6Al-4V. *Jom*, 73(6):1804–1818, 2021. ISSN 1543-1851.

M. Y. M. Londono. *On the Influence of Microstructural Features of Linear Friction Welding and Electron Beam Additive Manufacturing Ti-6Al-4V on Tensile and Fatigue Mechanical Properties*. Thesis, 2019. URL `https://dr.lib.iastate.edu/handle/20.500.12876/31927`.

G. Lütjering and J. C. Williams. *Titanium*. Springer, 2007. ISBN 3540730362.

B. Mannion and J. Heinzman. Plasma arc welding brings better control. *Tooling Prod*, 5:29–30, 1999.

F. Martina, P. A. Colegrove, S. W. Williams, and J. Meyer. Microstructure of interpass rolled wire+ arc additive manufacturing Ti-6Al-4V components. *Metallurgical and Materials Transactions A*, 46(12):6103–6118, 2015. ISSN 1543-1940.

M. Y. Mendoza, P. Samimi, D. A. Brice, B. W. Martin, M. R. Rolchigo, R. LeSar, and P. C. Collins. Microstructures and Grain Refinement of Additive-Manufactured Ti-xW Alloys. *Metallurgical and Materials Transactions A*, 48(7):3594–3605, 2017. ISSN 1073-5623 1543-1940. doi: 10.1007/s11661-017-4117-7.

M. Y. Mendoza, P. Samimi, D. A. Brice, I. Ghamarian, M. Rolchigo, R. LeSar, and P. C. Collins. On the role of composition and processing parameters on the microstructure evolution of Ti-xMo alloys. *BMC Chemistry*, 13(1), 2019. ISSN 2661-801X. doi: 10.1186/s13065-019-0529-3.

M. Y. Mendoza Londono. *Molten pool modeling, microstructure and grain refinement in Ti-alloys*. Thesis, 2016.

P. Mercelis and J. Kruth. Residual stresses in selective laser sintering and selective laser melting. *Rapid prototyping journal*, 2006. ISSN 1355-2546.

P. Michaleris and A. DeBiccari. Prediction of welding distortion. *Welding Journal-Including Welding Research Supplement*, 76(4):172s, 1997. ISSN 0043-2296.

R. P. Mudge and N. R. Wald. Laser engineered net shaping advances additive manufacturing and repair. *Welding Journal-New York-*, 86(1):44, 2007. ISSN 0043-2296.

P. Muller, G. Rückert, and P. Vinot. On the benefits of metallic additive manufacturing for propellers. In *Sixth International Symposium on Marine Propulsors smp'19, Rome, Italy*, number May, 2019.

NeoNickel. Titanium Titanium Alloy CategorisationNo Title, 2022. URL `https://www.neonickel.com/technical-resources/general-technical-resources/titanium-titanium-alloy-categorisation/`.

C. H. Ng, M. J. Bermingham, L. Yuan, and M. S. Dargusch. Towards β-fleck defect free additively manufactured titanium alloys by promoting the columnar to equiaxed transition and grain refinement. *Acta Materialia*, 224:117511, 2022. ISSN 1359-6454.

A. H. Nickel, D. M. Barnett, and F. B. Prinz. Thermal stresses and deposition patterns in layered manufacturing. *Materials Science and Engineering: A*, 317(1-2):59–64, 2001. ISSN 0921-5093.

J. Obielodan and B. Stucker. Characterization of LENS-fabricated Ti6Al4V and Ti6Al4V/TiC dual-material transition joints. *The International Journal of Advanced Manufacturing Technology*, 66(9-12):2053–2061, 2012. ISSN 0268-3768 1433-3015. doi: 10.1007/s00170-012-4481-9.

T. L. H. Office). WIRE ARC ADDITIVE MANUFACTURING (WAAM)., 2022. URL `https://www.twi-global.com/technical-knowledge/job-knowledge/arc-based-additive-manufacturing-137`.

Z. Pan, D. Ding, B. Wu, D. Cuiuri, H. Li, and J. Norrish. Arc welding processes for additive manufacturing: a review. *Transactions on intelligent welding manufacturing*, pages 3–24, 2018.

P. Peyre, P. Aubry, R. Fabbro, R. Neveu, and A. Longuet. Analytical and numerical modelling of the direct metal deposition laser process. *J. Phys. D: Appl. Phys.*, 41(2):25403, 2008. ISSN 0022-3727 1361-6463. doi: 10.1088/0022-3727/41/2/025403.

J. L. Prado-Cerqueira, J. L. Diéguez, and A. M. Camacho. Preliminary development of a wire and arc additive manufacturing system (WAAM). *Procedia Manufacturing*, 13:895–902, 2017. ISSN 2351-9789.

M. Qi, S. Huang, Y. Ma, S. S. Youssef, R. Zhang, J. Qiu, J. Lei, and R. Yang. Columnar to equiaxed transition during β heat treatment in a near β alloy by laser additive manufacture. *Journal of Materials Research and Technology*, 13:1159–1168, 2021. ISSN 2238-7854.

C. Qiu, G. A. Ravi, and M. M. Attallah. Microstructural control during direct laser deposition of a β-titanium alloy. *Materials Design*, 81:21–30, 2015. ISSN 02613069. doi: 10.1016/j.matdes.2015.05.031.

A. Queguineur, G. Rückert, F. Cortial, and J. Y. Hascoët. Evaluation of wire arc additive manufacturing for large-sized components in naval applications. *Welding in the World*, 62(2):259–266, 2018. ISSN 1878-6669.

M. J. Quintana, M. J. Kenney, P. Agrawal, and P. C. Collins. Texture analysis of additively manufactured Ti-6Al-4V deposited using different scanning strategies. *Metallurgical and Materials Transactions A*, 51(12):6574–6583, 2020. ISSN 1543-1940.

M. R. Rolchigo, M. Y. Mendoza, P. Samimi, D. A. Brice, B. Martin, P. C. Collins, and R. LeSar. Modeling of Ti-W Solidification Microstructures Under Additive Manufacturing Conditions. *Metallurgical and Materials Transactions A*, 48(7):3606–3622, 2017. ISSN 1073-5623 1543-1940. doi: 10.1007/s11661-017-4120-z.

N. A. Rosli, M. R. Alkahari, F. R. Ramli, S. Mat, and A. A. Yusof. Influence of process parameters on dimensional accuracy in GMAW based additive manufacturing. *Proceedings of Mechanical Engineering Research Day 2019*, 2019:7–9, 2019. ISSN 9672145659.

K. I. Schwendner, R. Banerjee, P. C. Collins, C. A. Brice, and H. L. Fraser. Direct laser deposition of alloys from elemental powder blends. *Scr. Mater.*, 45(10):1123–1129, 2001. ISSN 1359-6462.

J. W. Sears. The Effects of Processing Parameters on Microstructure and Properties of Laser Deposited PM Alloy 690N2 Powder. Report LM-02K021, Lockheed Martin Corporation, Schenectady, NY 12301 (US), 2002.

C. Shen, Z. Pan, D. Cuiuri, J. Roberts, and H. Li. Fabrication of Fe-FeAl functionally graded material using the wire-arc additive manufacturing process. *Metallurgical and Materials Transactions B*, 47(1):763–772, 2016. ISSN 1543-1916.

M. Simonelli, Y. Y. Tse, and C. Tuck. Effect of the build orientation on the mechanical properties and fracture modes of SLM Tiâ6Alâ4V. *Materials Science and Engineering: A*, 616:1–11, 2014.

S.Tamirisakandala, R. B. Bhat, and J. S. Tiley. Grain refinement of cast titanium alloys via trace boron addition—. *Scr. Mater*, 53(12):1421–1426, 2005.

M. Strantza, R. Ganeriwala, and B. Clausen. Effect of the scanning strategy on the formation of residual stresses in additively manufactured Ti-6Al-4V, 2021. URL `https://www.grandviewresearch.com/industry-analysis/3d-metal-printing-market#`.

J. D. Strickland. Applications of additive manufacturing in the marine industry. *Proceedings of PRADS2016*, 4:8th, 2016.

Q. Tan, Y. Yin, A. Prasad, G. Li, Q. Zhu, D. H. StJohn, and M.-X. Zhang. Demonstrating the roles of solute and nucleant in grain refinement of additively manufactured aluminium alloys. *Additive Manufacturing*, 49:102516, 2022. ISSN 2214-8604.

S. N. Tedman-Jones, S. D. McDonald, M. J. Bermingham, D. H. StJohn, and M. S. Dargusch. A new approach to nuclei identification and grain refinement in titanium alloys. *Journal of Alloys and Compounds*, 794:268–284, 2019. ISSN 0925-8388.

L. Thijs, F. Verhaeghe, T. Craeghs, J. V. Humbeeck, and J.-P. Kruth. A study of the microstructural evolution during selective laser melting of Tiâ6Alâ4V. *Acta Mater.*, 58(9):3303–3312, 2010. ISSN 13596454. doi: 10.1016/j.actamat.2010.02.004.

F. Wang, S. Williams, P. Colegrove, and A. A. Antonysamy. Microstructure and Mechanical Properties of Wire and Arc Additive Manufactured Ti-6Al-4V. *Metall. Mater. Trans. A*, 44(2): 968–977, 2012. ISSN 1073-5623 1543-1940. doi: 10.1007/s11661-012-1444-6.

X. Wang, L.-J. Zhang, J. Ning, S. Li, L.-L. Zhang, and J. Long. Hierarchical grain refinement during the laser additive manufacturing of Ti-6Al-4V alloys by the addition of micron-sized refractory particles. *Additive Manufacturing*, 45:102045, 2021. ISSN 2214-8604.

C. Xiaolong, L. Zulei, G. Yanhua, S. Zhonggang, W. Yaoqi, and Z. Lian. A study on the grain refinement mechanism of Ti-6Al-4V alloy produced by wire arc additive manufacturing using hydrogenation treatment processes. *Journal of Alloys and Compounds*, 890:161634, 2022. ISSN 0925-8388.

M. Yakout, M. A. Elbestawi, and S. C. Veldhuis. A study of the relationship between thermal expansion and residual stresses in selective laser melting of Ti-6Al-4V. *Journal of Manufacturing Processes*, 52:181–192, 2020. ISSN 1526-6125.

Y. Z. Zhang, C. Meacock, and R. Vilar. Laser powder micro-deposition of compositional gradient TiâCr alloy. *Materials Design*, 31(8):3891–3895, 2010. ISSN 02613069. doi: 10.1016/j.matdes.2010.02.052.

Y. Zhu, X. Tian, J. Li, and H. Wang. The anisotropy of laser melting deposition additive manufacturing Tiâ6.5 Alâ3.5 Moâ1.5 Zrâ0.3 Si titanium alloy. *Materials Design*, 67:538–542, 2015. ISSN 0261-3069.

M. Ziółkowski and T. Dyl. Possible applications of additive manufacturing technologies in shipbuilding: a review. *Machines*, 8(4):84, 2020.